nature astronomy

ARTICLES

DOI: 10.1038/s41550-017-0228-8

Corrected: Publisher correction

# Hydrogen-rich supernovae beyond the neutrino-driven core-collapse paradigm

G. Terreran[1,2,3*], M. L. Pumo[2,4,5], T.-W. Chen[6], T. J. Moriya[7], F. Taddia[8], L. Dessart[9], L. Zampieri[2], S. J. Smartt[1], S. Benetti[2], C. Inserra[1], E. Cappellaro[2], M. Nicholl[10], M. Fraser[11], Ł. Wyrzykowski[12], A. Udalski[12], D. A. Howell[13,14], C. McCully[13,14], S. Valenti[15], G. Dimitriadis[16], K. Maguire[1], M. Sullivan[16], K. W. Smith[1], O. Yaron[17], D. R. Young[1], J. P. Anderson[18], M. Della Valle[19,20], N. Elias-Rosa[2], A. Gal-Yam[17], A. Jerkstrand[21], E. Kankare[1], A. Pastorello[2], J. Sollerman[8], M. Turatto[2], Z. Kostrzewa-Rutkowska[12,22,23], S. Kozłowski[12], P. Mróz[12], M. Pawlak[12], P. Pietrukowicz[12], R. Poleski[12,24], D. Skowron[12], J. Skowron[12], I. Soszyński[12], M. K. Szymański[12] and K. Ulaczyk[12,25]

**Type II supernovae are the final stage of massive stars (above 8 $M_{\odot}$) which retain part of their hydrogen-rich envelope at the moment of explosion. They typically eject up to 15 $M_{\odot}$ of material, with peak magnitudes of −17.5 mag and energies in the order of $10^{51}$ erg, which can be explained by neutrino-driven explosions and neutron star formation. Here, we present our study of OGLE-2014-SN-073, one of the brightest type II supernovae ever discovered, with an unusually broad lightcurve combined with high ejecta velocities. From our hydrodynamical modelling, we infer a remarkable ejecta mass of $60^{+42}_{-16}$ $M_{\odot}$ and a relatively high explosion energy of $12.4^{+13.0}_{-5.9} \times 10^{51}$ erg. We show that this object belongs, along with a very small number of other hydrogen-rich supernovae, to an energy regime that is not explained by standard core-collapse neutrino-driven explosions. We compare the quantities inferred by the hydrodynamical modelling with the expectations of various exploding scenarios and attempt to explain the high energy and luminosity released. We find some qualitative similarities with pair-instability supernovae, although the prompt injection of energy by a magnetar seems to be a viable alternative explanation for such an extreme event.**

Type II supernovae explode energetically and brightly[1] and leave behind a neutron star[2]. One particular type II supernova, OGLE-2014-SN-073 (hereafter referred to as OGLE14-073), was discovered in phase IV of the Optical Gravitational Lensing Experiment (OGLE-IV) transient search[3,4] on 2014 August 15.43 universal time (UT) at coordinates $\alpha_{J2000} = 05\,\mathrm{h}\,28\,\mathrm{m}\,51.61\,\mathrm{s}$, $\delta_{J2000} = -62°\,20'\,16.05''$. No stringent constraint on the explosion epoch could be placed, with the last non-detection around 110 d before discovery. A classification spectrum taken on 2014 September 24.28 UT (ref. [5]) by the Public European Southern Observatory (ESO) Spectroscopic Survey of Transient Objects (PESSTO; ref. [6]) showed very prominent hydrogen P Cygni features and no signs of an interaction between the ejecta and circumstellar medium. Despite the fact that the spectrum was taken around 40 d after discovery, the temperature and velocities inferred best matched a type II supernova around 15 d after explosion, posing a problem for the determination of the actual age of the event.

## Host galaxy

Although OGLE14-073 appeared hostless, a pre-discovery image taken on 2012 December 22.33 UT by the Dark Energy Survey (DES; ref. [7]) during Science Verification showed a faint galaxy at

[1]Astrophysics Research Centre, School of Mathematics and Physics, Queen's University Belfast, Belfast BT7 1NN, UK. [2]INAF - Osservatorio Astronomico di Padova, Vicolo dell'Osservatorio 5, 35122 Padova, Italy. [3]Dipartimento di Fisica e Astronomia G. Galilei, Università di Padova, Vicolo dell'Osservatorio 3, 35122 Padova, Italy. [4]Dipartimento di Fisica e Astronomia, Università degli studi di Catania, Via Santa Sofia 64, 95123 Catania, Italy. [5]INFN - Laboratori Nazionali del Sud, Via Santa Sofia 62, 95123 Catania Italy. [6]Max-Planck-Institut für Extraterrestrische Physik, Giessenbachstraß e 1, 85748 Garching, Germany. [7]Division of Theoretical Astronomy, National Astronomical Observatory of Japan, National Institutes of Natural Sciences, 2-21-1 Osawa, Mitaka, Tokyo 181-8588, Japan. [8]The Oskar Klein Centre, Department of Astronomy, Stockholm University, AlbaNova, 10691 Stockholm, Sweden. [9]Unidad Mixta Internacional Franco-Chilena de Astronomía (CNRS UMI 3386), Departamento de Astronomía, Universidad de Chile, Camino El Observatorio 1515, Las Condes, Santiago, Chile. [10]Harvard-Smithsonian Center for Astrophysics, 60 Garden Street, Cambridge, MA 02138, USA. [11]School of Physics, O'Brien Centre for Science North, University College Dublin, Belfield, Dublin 4, Ireland. [12]Warsaw University Observatory, Al. Ujazdowskie 4, 00-478 Warszawa, Poland. [13]Las Cumbres Observatory, 6740 Cortona Drive Suite 102, Goleta, CA 93117, USA. [14]Department of Physics, University of California, Santa Barbara, Broida Hall, Mail Code 9530, Santa Barbara, CA 93106-9530, USA. [15]Department of Physics, University of California, Davis, CA 95616, USA. [16]Department of Physics and Astronomy, University of Southampton, Southampton SO17 1BJ, UK. [17]Department of Particle Physics and Astrophysics, Weizmann Institute of Science, Rehovot 76100, Israel. [18]European Southern Observatory, Alonso de Córdova 3107, Casilla 19, Santiago, Chile. [19]INAF - Osservatorio Astronomico di Capodimonte, Salita Moiariello 16, 80131 Napoli, Italy. [20]International Center for Relativistic Astrophysics, Piazza delle Repubblica, 10, 65122 Pescara, Italy. [21]Max-Planck-Institut fur Astrophysik, Karl-Schwarzschild-Str. 1, D-85741 Garching, Germany. [22]SRON Netherlands Institute for Space Research, Sorbonnelaan 2, 3584 CA Utrecht, The Netherlands. [23]Department of Astrophysics, Institute for Mathematics, Astrophysics and Particle Physics, Radboud University Nijmegen, PO Box 9010, 6500 GL Nijmegen, The Netherlands. [24]Department of Astronomy, Ohio State University, 140 West 18th Avenue, Columbus, OH 43210, USA. [25]Department of Physics, University of Warwick, Gibbet Hill Road, Coventry CV4 7AL, UK.
*e-mail: gterreran01@qub.ac.uk

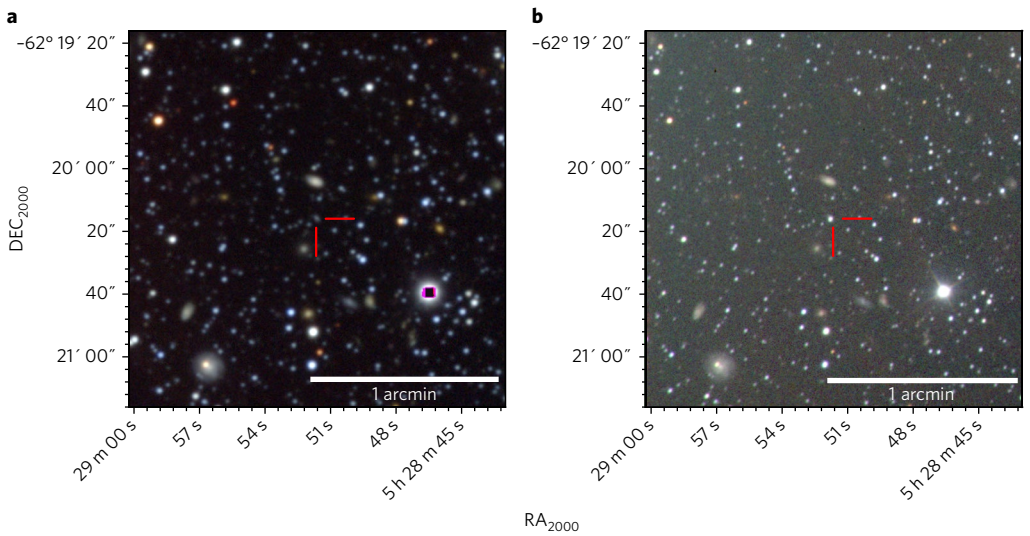


**Fig. 1 | RGB images of the OGLE14-073 field. a**, Pre-explosion image taken on 2012 December 22.33 UT by the DES during Science Verification. Sloan Digital Sky Survey gri filters have been used. At the position of OGLE14-073, marked in red, the faint anonymous host galaxy is observed. **b**, Post-explosion image taken on 2014 September 24.29 UT by PESSTO with the NTT and ESO Faint Object Spectrograph and Camera (version 2). Johnson–Cousins BVR filters have been used.

the position of the supernova (Fig. 1a). The magnitudes of the host were measured on the available griz-band images using aperture photometry within DAOPHOT (see Methods). We inferred $m_g = 23.04 \pm 0.10$ mag, $m_r = 21.81 \pm 0.16$ mag, $m_i = 21.98 \pm 0.13$ mag and $m_z = 21.36 \pm 0.23$ mag. From this observed photometry, we estimated the stellar mass of the host galaxy. We used the stellar population model programme Multi-wavelength Analysis of Galaxy Physical Properties (MAGPHYS; ref. [8]), which provided a stellar mass of $\log M = 8.7\ M_\odot$ and a $1\sigma$ range from 8.5 to $8.9\ M_\odot$ for the host of OGLE14-073. This was a few times larger than that of the typical mass of the host galaxies of superluminous supernovae with slowly fading lightcurves[9]. Following the mass–metallicity relation, this implies a moderately sub-solar metallicity for the host of OGLE14-073.

A strong contamination from the host galaxy was clearly visible in our last spectrum (see Fig. 2a). From these narrow emissions we could measure a redshift of $z = 0.1225$, and from the ratio between H$\alpha$ and [N II] lines[10], we inferred an oxygen abundance of $12 + \log(\mathrm{O/H}) = 8.36 \pm 0.10$ for the host galaxy of OGLE14-073, which is half of the solar abundance. This estimate, together with the stellar mass previously inferred, is in good agreement with the mass–metallicity relation[11].

## Spectrophotometric evolution

At a measured redshift of $z = 0.1225$, OGLE14-073 peaked at −19 mag in the I-band. Very few non-interacting type II supernovae have a luminosity comparable to OGLE14-073. The roughly three month rise to maximum shown by OGLE14-073 (Fig. 3 and Supplementary Information) and the broad peak of the lightcurve resemble the peculiar type II supernova SN 1987A (ref. [12]); however, SN 1987A was much fainter. After a steep post-maximum decline, the lightcurve of OGLE14-073 settles onto a tail consistent with the decay rate of $^{56}$Co. From the luminosity of this tail, the amount of $^{56}$Ni synthesized during the explosion can be inferred. This estimate requires an assumption of the explosion epoch, which is not well constrained. However, if we consider that the explosion occurred only one day before discovery, we can derive a solid lower limit $M_{\mathrm{Ni}} \geq 0.47 \pm 0.02\ M_\odot$, which is the largest $M_{\mathrm{Ni}}$ ever estimated for a hydrogen-rich supernova[13]. Overall, the spectroscopic evolution of OGLE14-073 (Fig. 2a) is much slower compared with other type II supernovae (Fig. 2b), with almost no evolution during roughly 160 d of spectroscopic follow-up. The spectra are dominated by hydrogen and iron-group elements throughout the entire spectral sequence. Weak forbidden lines start to appear only in the last spectrum 115 d after the maximum. Despite the slow spectroscopic evolution, a progressive cooling of the temperature is visible, as well as a redward shift of the minima of the main absorption features (see Supplementary Information).

## Lightcurve modelling

To investigate the nature of OGLE14-073, we used the well-tested modelling procedure described in ref. [14], which has already been applied to several other type II supernovae (see Methods for a detailed description). First, an exploratory analysis was conducted to determine the parameter space. This was done using the semi-analytical code developed by ref. [15]. The outcomes from this preliminary examination set the framework for the more sophisticated hydrodynamical modelling; that is, the general-relativistic, radiation-hydrodynamics Lagrangian code presented in ref. [16]. The best fit was obtained by simultaneously comparing (using a chi-squared test) the bolometric lightcurve, photospheric gas velocity and continuum temperature of OGLE14-073 with the corresponding quantities simulated by the code. The resulting best model (as shown in Fig. 4) had an explosion energy $E = 12.4^{+13.0}_{-5.9} \times 10^{51}$ erg, an ejected mass $M_{\mathrm{ej}} = 60^{+42}_{-16}\ M_\odot$ and a radius at explosion $R_0 = 3.8^{+0.8}_{-1.0} \times 10^{13}$ cm ($1\sigma$ confidence level). In the standard core-collapse paradigm, the energy of the explosion results from neutrino deposition after neutron star formation[17]. Given the low cross-section of the neutrino-matter interaction, these are assumed to deposit only around 1% of their energy in the ejecta, leading to a fairly robust energy upper limit of $E \lesssim 2 \times 10^{51}$ erg (ref. [2]). Therefore, to achieve the $E \gtrsim 10^{52}$ erg inferred for OGLE14-073 in the context of neutrino-driven explosions, one has to invoke a much higher, and possibly unphysical, neutrino deposition fraction. In addition, the $M_{\mathrm{ej}}$ inferred is several times higher than typical values for type II supernovae[13,18]. We stress that the models were calculated assuming that the supernova exploded the day before discovery. However, given the lack of constraints, it is legitimate to assume that the supernova actually exploded well before discovery, and moving the explosion epoch back in time the energy, ejecta mass and Ni mass accordingly. Therefore these are all to be considered to be lower limits. It is

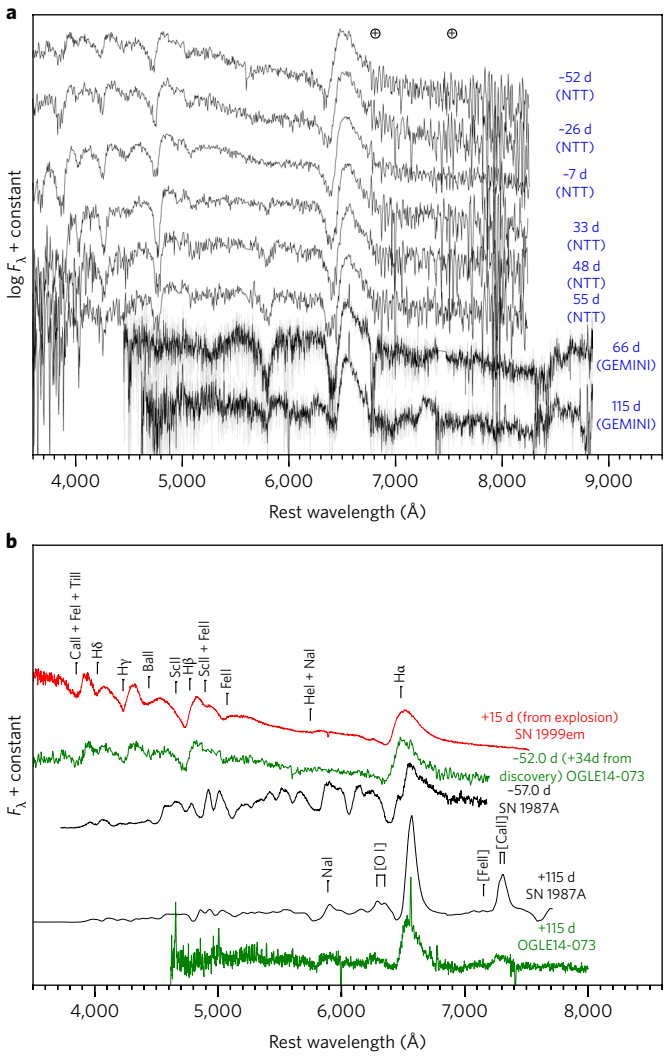


**Fig. 2 | Optical spectral evolution of OGLE14-073 and comparison with SN 1987A. a**, Optical spectral evolution of OGLE14-073. The spectra are corrected for reddening and redshift, and shifted vertically for better display. On the right of each spectrum, the phase (in the rest frame) with respect to the bolometric maximum lightcurve and the telescope used are reported. The two GEMINI spectra are smoothed with a boxcar of five pixels. The positions of the telluric $O_2$ A and B absorption bands are marked with the ⊕ symbol. All spectra are available at http://wiserep.weizmann.ac.il/home. **b**, Spectroscopical comparison between OGLE14-073 and SN 1987A, given the similarities between their lightcurves. On the right of each spectrum, the phase with respect to the bolometric maximum epoch is reported, unless differently specified. For comparison, the spectrum of SN 1999em 15 d after the explosion is also shown, which was the best match for the classification spectrum. See Supplementary Information for the references of the objects used for the comparison.

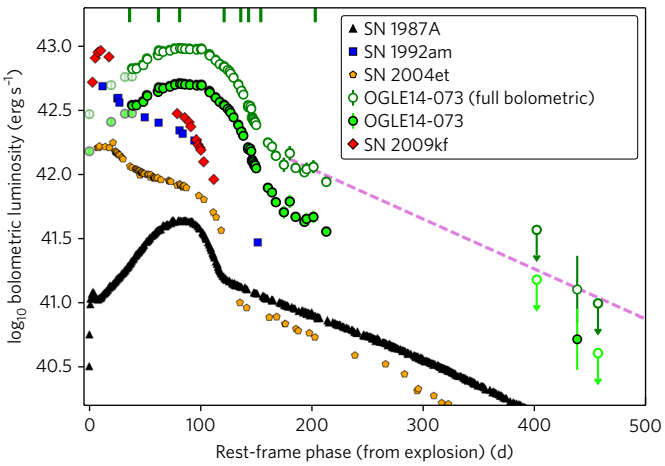


**Fig. 3 | Bolometric lightcurve of OGLE14-073 and comparison with other type II supernovae.** Comparison of the optical pseudo-bolometric lightcurve of OGLE14-073 with other luminous non-interacting type II supernovae (the type II-P supernovae SN 1992am, SN 2004et and SN 2009kf, and the peculiar SN 1987A; see Supplementary Information for references). The phase is in the rest frame and from the explosion for all the supernovae apart from OGLE14-073, for which the first detection was used. The initial four points of OGLE14-073 (shaded) were calculated from only one I band image per epoch, assuming the same spectral energy distribution as for the first epoch with multi-band information. For comparison we have included the full-bolometric lightcurve of OGLE14-073 (see Methods). The dashed magenta line marks the slope of the $^{56}$Co decay. The green lines at the top of the frame mark the epochs at which the spectra were measured.

difficult to reconcile the extraordinary energetics of OGLE14-073, together with its high $M_{ej}$ and $M_{Ni}$ values, with the conventional core-collapse scenario.

## Pair-instability scenario

If the progenitor of OGLE14-073 was a very massive star (with a helium core between 64 and 133 $M_\odot$; ref. [19]), it could have ended its life due to the instabilities induced by the production of $e^+e^-$ pairs in a pair-instability supernova (PISN). These events are characterized by very bright (up to $10^{44}$ erg s$^{-1}$) and broad lightcurves, with rise times $\gtrsim$150 d, due to large ejecta masses and, hence, very long diffusion times[20,21]. In Fig. 5, we compare the lightcurve of OGLE14-073 with those of hydrogen-rich PISN models from ref. [20]. In particular, we consider a progenitor with a zero-age main-sequence (ZAMS) mass $M_{ZAMS} = 190\,M_\odot$ (helium core: ~100 $M_\odot$), as among the models of ref. [20], they produced the dimmest lightcurves (still brighter than OGLE14-073). Both lightcurves coming from a red supergiant and a blue supergiant progenitor are considered. The red supergiant model is brighter at early phases and lacks the observed rise-time of OGLE14-073. The decline phase has a very similar slope to that of OGLE14-073. The blue supergiant progenitor lightcurve shows a reasonable qualitative match; however, we lack data before −100 days to probe the full rise (and early peak). OGLE14-073 experiences a faster decline over the first 80 d after the peak, but in the tail phase shows similar decline rates to the red supergiant model. The tail phase luminosities (Fig. 5) indicate that the $^{56}$Ni mass in the two PISN models is much higher than in OGLE14-073. Our initial estimate of $M_{Ni} \geq 0.47\,M_\odot$ is below the values of 2.6–3.0 $M_\odot$ of the models. However, we lack a constraint on the explosion epoch of OGLE14-073, and if we assume that the explosion occurred ~90 d before the initial discovery, $M_{Ni}$ could be as high as ~1.1 $M_\odot$. While this is still low, it is in the regime of PISN events arising from less massive progenitors (helium cores: $\lesssim$90 $M_\odot$; ref. [19]). The pre-maximum spectra of the PISN models of ref. [20] show many similarities with OGLE14-073, being dominated by the Balmer lines. However, the models show the hydrogen disappearing after the peak. This occurs because at the time of the explosion the progenitors of PISN have very massive helium cores, which prevent the centrally distributed $^{56}$Ni from being mixed with the outer ejecta, where the hydrogen is mainly situated. Instead, in OGLE14-073, the hydrogen dominates the spectrum at all epochs. Therefore, despite the similarities with the models (see also Supplementary Fig. 4 for a comparison of temperatures and velocities), the late-time spectra of OGLE14-073 are in

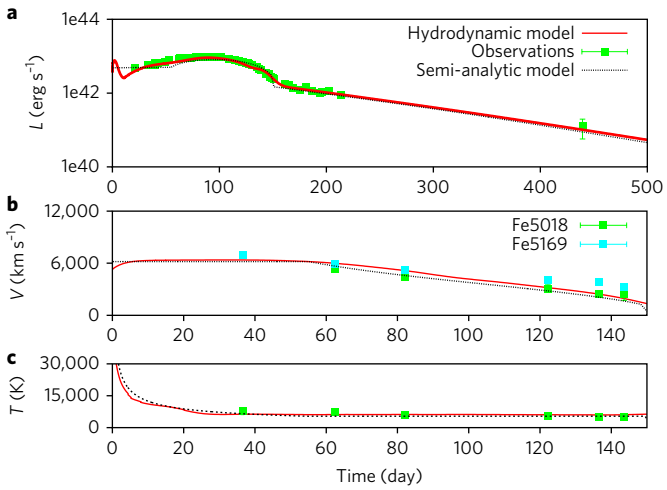


**Fig. 4 | Hydrodynamical modelling of OGLE14-073.** Comparison of the evolution of the main observables of OGLE14-073 with the best-fitting model computed with the general-relativistic, radiation-hydrodynamics code described in ref. [16]. The best-fitting model parameters are $E=12.4\times10^{51}$ erg, $M_{ej}=60\,M_{\odot}$ and $R_0=3.8\times10^{13}$ cm. **a**, Bolometric light curve. **b**, Photospheric velocity. **c**, Photospheric temperature evolution. We assume the explosion occurred the day before discovery, and the phase is referred to this epoch. To estimate the photospheric temperature and velocity from the observations, we respectively used the continuum temperature and the minima of the profile of the Fe lines, which are considered good tracers of the photospheric velocity in type II supernovae. For the sake of completeness, the best-fitting model, computed with the semi-analytical code[15] ($E=21\times10^{51}$ erg, $M_{ej}=69\,M_{\odot}$ and $R_0=3.5\times10^{13}$ cm), is also shown.

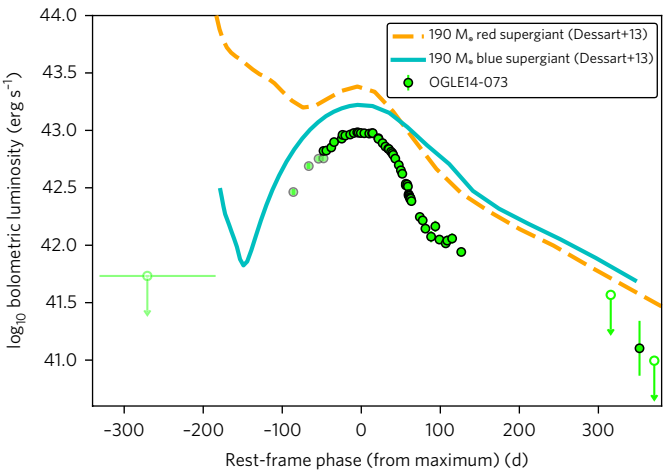


**Fig. 5 | Comparison of the lightcurve of OGLE14-073 with PISN models.** The green circles mark the bolometric lightcurve of OGLE14-073. Model lightcurves of PISN, arising from a blue supergiant and a red supergiant progenitor are also shown[20], both with a $M_{ZAMS}$ value of 190 $M_{\odot}$. With the mass-loss prescriptions they used and assuming a metallicity of $10^{-4}\,Z_{\odot}$, all their models encountered the pair instability when the star was a red supergiant. The blue supergiant model was produced by artificially truncating the hydrogen envelope just before the explosion to simulate stronger mass loss. The leftmost point is an upper limit measured from the stack image of all the non-detections (provided by OGLE) available in the span of time marked by the horizontal bar.

conflict with a PISN interpretation (unless a source other than $^{56}$Ni is ionising the hydrogen).

Alternatively, in progenitors with smaller helium cores than those of PISN (that is, ~30–60 $M_{\odot}$), the instabilities arising from the creatio of pairs could be insufficient to disrupt the entire star, but violent enough to expel part of the envelope[22]. The interaction due to the collision between two (or more) of these shells of material could be an efficient way to power luminous lightcurves, in a so-called pulsational PISN (ref. [22]). If the shells are dense and massive enough, a photosphere could be created, which could mimic a normal supernova, without clear signs of interaction from the spectra. Given the broad lightcurve of OGLE14-073 and the hydrogen lines visible at all epochs, a scenario with a fast, low-mass inner shell interacting with a slower massive outer one (for example, see SN 1994W; ref. [23]) could perhaps reproduce the observables. Assuming the light curve rise-time to be the diffusion time $t_d$ in the shell, an opacity $\kappa=0.34\,\mathrm{cm^2\,g^{-1}}$, an outer radius $R\sim10^{16}$ cm and a constant density $\rho$, using $t_d=\kappa\rho R^2/c$ (ref. [24]) we get $M_{shell}\sim14\,M_{\odot}$. Therefore, the outer shell should have a kinetic energy in the order of $10^{52}$ erg. Similar energies can indeed be produced in the most extreme pulsational PISN (ref. [22]). However, in most models, such energies are achieved through large masses and relatively low velocities (~1,000–2,000 km s$^{-1}$), while the first spectrum of OGLE14-073 shows the minimum of the absorption of H$\alpha$ at ~10,000 km s$^{-1}$, which is probably too high for a pulsation event due to pair instabilities. Note, in addition, that in this scenario the progenitor star might still be alive, and there would be no $^{56}$Ni synthesized, thus the tail phase match with the radioactive decay of $^{56}$Co would be coincidental.

## Hypernova scenario

We may notice that, although rare, supernovae with $E>10^{52}$ erg do exist. Historically, they have been labelled as 'hypernovae', and some are associated with long gamma-ray bursts; for example, SN 1998bw (ref. [25]). Moreover, a hypernova-like explosion has also been invoked to explain the luminous type II-P supernova SN 2009kf (refs [26,27]). In the case of SN 2009kf, the following parameters were inferred: $M_{ej}=28\,M_{\odot}$, $E=22\times10^{51}$ erg and $M_{Ni}=0.40\,M_{\odot}$. These values are not far from those found for OGLE14-073 (although inferred with a fairly different methodology) and the spectra also show similarities[26]. However, the lightcurves are quite different (see Fig. 3), with that of SN 2009kf resembling more normal type II-P supernovae. To try to associate such energetic events within a known scenario, we built a sample of normal type II supernovae, long-rising 1987A-like supernovae, standard Ibc supernovae (stripped-envelope) and hypernovae, for which estimates of $E$ and $M_{ej}$ were available[18,28,29], and we plotted these parameters in Fig. 6a (we point out that given the different sources, the methods applied to infer the parameters are quite heterogeneous). The transients appear to gather in four clusters. In particular, OGLE14-073 sits in a region characterized by both high $E$ and high $M_{ej}$, together with SN 2009kf and also with two long-rising supernovae, SN 2004ek and SN 2004em. This domain of the plot is not populated by 'traditional' transients. Indeed, the ejecta of these four supernovae are much larger than those of the hypernovae and are much more energetic than canonical type II events. Such clustering disappears when comparing $E$ with $M_{Ni}$ (Fig. 6b). Here, there seems to be a continuum, with $M_{Ni}$ increasing with $E$, a trend already reported in previous studies[30,31]. OGLE14-073 follows the general tendency; however, it sits far from all other type II supernovae (with the exception of SN 2009kf) in a region populated by hypernovae. Given the scarcity of the sample, we cannot exclude the possibility that high-energy type II supernovae may somehow extend towards lower energies or masses, implying that this would either require a much more efficient core-collapse mechanism, or much larger hydrogen-rich progenitors for hypernovae.

To explain the high-energy properties of hypernovae, an additional source powering the explosion is required. Such a source is

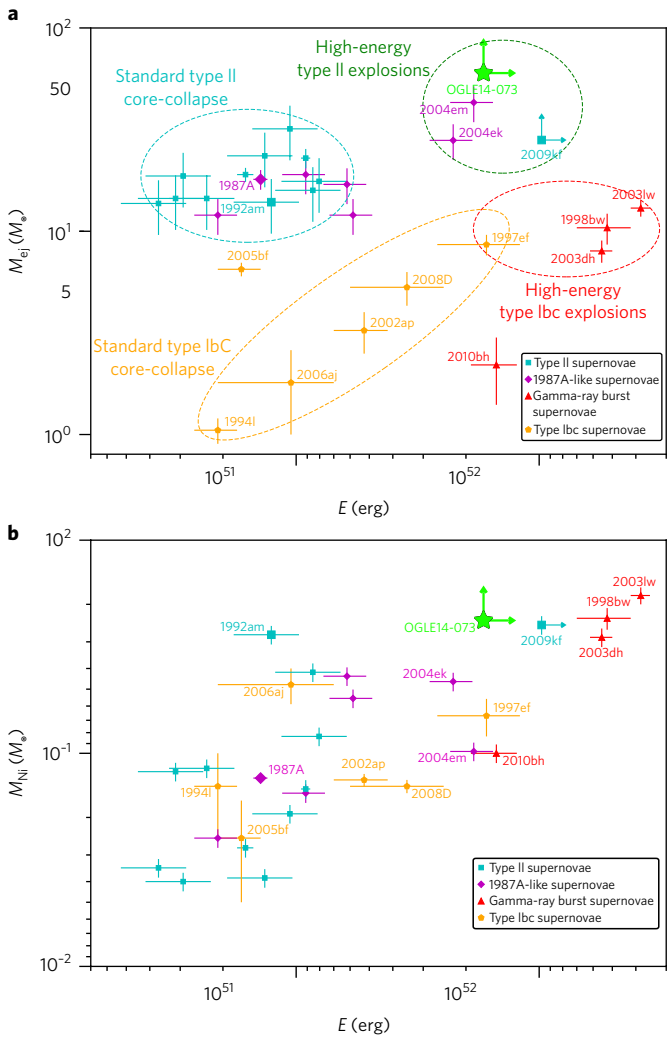


**Fig. 6 | Ejecta mass versus explosion energy and $^{56}$Ni mass plots.** **a**, Ejecta mass $M_{ej}$ versus explosion energy $E$ plot. A sample of 'normal' type II supernovae[18], 1987A-like supernovae[28], type Ibc supernovae and supernovae related with gamma-ray bursts (hypernovae[29]) are shown. Four major groups are identified in the graph, with OGLE14-073 sitting in a new region of high-energy type II supernovae, together with the supernovae SN 2004ek, SN 2004em and SN 2009kf. This group of hydrogen-rich supernovae appears as a separate cluster from the other standard core-collapse supernovae, suggesting a different explosion mechanism for this type of energetic transient. **b**, Explosion energy E versus $^{56}$Ni mass $M_{Ni}$ plot. A continuum of events is evident, with more energetic events synthesizing more $^{56}$Ni. This tendency has already been found in several other studies[30], which led to the claim of a unique exploding mechanism for all the classes of supernovae considered, invoking collapse-induced thermonuclear explosions as an alternative to neutrino-driven explosions[31]. OGLE14-073 seems to respect the general trend, but it sits far from the other hydrogen-rich events (with the exception of SN 2009kf).

usually identified in an 'inner engine', in the form of a magnetar (for example, ref. [32]) or a black hole (for example, ref. [33]). In the first case, a protoneutron star born with a spin period in the order of 1 ms and a magnetic field in the order of $10^{15}$ G can inject $10^{52}$ ergs of energy in the inner ejecta on a time scale of 10–100 s. This energetic shock soon reaches the slower supernova shock, while still travelling through the envelope of the progenitor star, boosting it and producing a hyperenergetic supernova explosion[32]. Such an energetic shock also has a deep influence on nucleosynthesis, as a nickel excess is also expected. Note that this magnetar engine is different from that supposed to sustain the lightcurves of superluminous supernovae[34,35], as in those cases the magnetic field of the neutron star is one order of magnitude lower, injecting energies of ~$10^{51}$ erg on a timescale of days to weeks[36]. We can speculate that a magnetar with $B \geq 10^{15}$ G and a spin period of ~1 ms could be hidden at the centre of the explosion of OGLE14-073, and this could be the source of energy of the most powerful hydrogen-rich supernovae shown in Fig. 6. Alternatively, the inner engine could comprise a rapidly rotating black hole, which—as a consequence of the accretion of the matter in-falling from the collapsing progenitor—launches relativistic jets, triggering the explosion.

## Conclusions

Regardless of the energy injection mechanism, the shape of the lightcurve and the spectra of OGLE14-073 unequivocally point to the presence of a massive hydrogen envelope, which is also confirmed by our hydrodynamical modelling. Despite the uncertainties regarding a definitive determination of the explosion scenario, it appears certain that the progenitor was much larger than the typical progenitors of type II supernovae[37]. However, explosion energies in the order of $10^{52}$ erg and ejecta masses above 50 $M_\odot$ are too high for a canonical core-collapse supernova and neutrino-driven explosion. Although there are few other high-energetic hydrogen-rich events that seem to defy the standard core-collapse scenario, OGLE14-073 appears to have an unmatched spectrophotometric evolution. It is puzzling how the progenitor managed to retain such a big amount of its outer envelope without triggering mass-loss events and transitioning to a luminous blue variable or a Wolf–Rayet star[38]. Indeed, progenitors in the mass range that we infer from the ejecta mass should explode as hydrogen-free supernovae, according to the current state-of-the-art models. Perhaps a low metallicity environment, as our host galaxy analysis suggested, could have suppressed the mass loss[39]. In this context, PISN are supposed to come from massive population III progenitors; however, both the PISN and the pulsational PISN scenarios have inconsistencies with the observables of OGLE14-073. We argued that a central engine scenario could in principle provide the energy shown by OGLE14-073, but this leads to other issues, such as how and why some stars are able to produce compact objects with ultra-intense magnetic fields while others do not. Moreover, it is not clear how these peculiar neutron stars (or black holes) interact with massive envelopes, especially if jets form, influencing the geometry of the explosion, $^{56}$Ni mixing and radiation transport. Together, we believe that the observables of OGLE14-073 provide strong motivation for the search for other similar objects (possibly with better explosion epoch constraints) and more detailed modelling.

## Methods

**Follow-up and data reduction.** OGLE-IV reported the discovery of OGLE14-073 on 2014 September 20.32 UT (ref. [3]), with an I band magnitude of ~19.5 mag. However, inspection of the acquisition images close to the discovery revealed a couple of previous detections, the earliest being on 2014 August 15.43 UT. We used this date as the discovery reference throughout the paper. The last non-detection is from OGLE-IV, on 2014 April 27.98 UT (limit 20.0 mag in I band), around 110 d before the first detection. The observational campaign of OGLE14-073 lasted for about eight months, before it went behind the Sun. Then, when it was visible again, we were able to obtain just one more detection (S/N~4), in addition to a number of upper limits. The photometric campaign has also been supported by the acquisition of eight spectra. Supplementary Table 1 lists the telescopes and instrumentation involved in the follow-up of OGLE14-073.

Images from the Las Cumbres Observatory[40] and OGLE-IV were automatically ingested and reduced using the lcogtsnpipe pipeline[41] and the OGLE-IV data analysis system[4], respectively. We reduced all the images coming from the other telescopes by correcting for overscan, bias and flatfields, using standard procedures within the Image Reduction and Analysis Facility (IRAF). The near-infrared images, all of which came from the infrared spectrograph and imaging camera Son of ISAAC (SOFI) on the ESO's New Technology Telescope (NTT), were reduced using the PESSTO pipeline[6]. For the photometric measurements,

the SNOoPY package[42] was used, which allowed—for each exposure—the extraction of the magnitude of the supernova with the point spread function fitting technique, using DAOPHOT (ref. [43]). If the transient was not detected in the image, conservative upper limits were estimated, corresponding to an S/N of 2.5. To derive the magnitude of the supernova, we first estimated the zero point and the colour term of the night through the observation of photometric standard fields[44]. Then, we calibrated a sequence of secondary stars in the field of OGLE14-073, which were subsequently used to calibrate the supernova in each night. For near-infrared images, we used the Two Micron All Sky Survey catalogue[45] as a reference for the calibration. Finally, we applied a *K*-correction computed from the sequence of spectra we gathered. Error estimates were obtained through an artificial star experiment, combined (in quadrature) with the point spread function fit error returned by DAOPHOT, and the propagated errors from the photometric calibration. Sloan Digital Sky Survey griz filters were used in three epochs taken at Las Cumbres Observatory, and we converted the extracted magnitudes to Johnson–Cousins BVRI filters, following the relations derived by ref. [46]. The *i* filter of the ESO Faint Object Spectrograph and Camera (version 2; EFOSC2) is actually a Gunn *i*; nevertheless, it has been calibrated as a Cousins *I*. All the magnitudes reported in this work have been calibrated in the Vega system. OGLE-IV provided a great number of images in which the supernova was not detectable (both pre-explosion images and images taken after the supernova faded below their detection limit). We stacked them in three deeper images, one of which showed a detection.

Given the contamination of the galaxy in the last epochs, a template subtraction would be appropriate. However, the pre-discovery images were either not deep enough (the ones from OGLE) or had different filters from those used for the follow-up (the one from the DES). The supernova was not detected in the very last epoch taken with the visual and near UV FOcal Reducer and low dispersion Spectrograph (version 2; FORS2) on the ESO's Very Large Telescope (VLT) using VRI-band filters, so we decided to use this last acquisition as the template. We performed the subtraction using hotpants (http://www.astro.washington.edu/users/becker/v2.0/hotpants.html) by point spread function matching of the field stars. We note that the epoch used as a template was taken only 75 d after the last detection in the R and I bands. Thus, it is likely that the supernova flux was not completely negligible yet, resulting in an over-subtraction of the actual supernova signal. For this reason, the magnitude measurements at 400 d in the R and I bands are to be considered as upper limits.

The bolometric and pseudo-bolometric luminosity lightcurves of OGLE14-073 were calculated by integrating the spectral energy distribution (SED) using the trapezoidal rule. Each photometric point is converted in flux at the wavelength equal to the effective wavelength of the filter. All the points are then connected to form a very low-resolution SED. The blue- and red-most points are also extended by half of the effective width of the corresponding filter, with zero flux assumed outside these boundaries. Finally, the obtained SED is integrated by summing the area of the trapezoids that comprise it. Since our photometry mainly covered the optical wavelengths, we had to apply a bolometric correction to create a full bolometric lightcurve. We estimated this by fitting the spectral energy distribution (to estimate the bolometric correction we used only the spectral energy distribution measured from epochs where the supernova was detected in more than two bands) with a blackbody and then adding the missing flux, measured from 0 to $\infty$, to the optical luminosities.

For the optical spectra, the extractions were performed using standard IRAF routines. The spectra of comparison lamps and standard stars acquired on the same night and with the same instrumental setting were used for the wavelength and flux calibrations, respectively. A cross-check of the flux calibration with the photometry (if available from the same night) and removal of the telluric bands with the standard star were also applied. The GEMINI spectra were reduced using a combination of the Gemini IRAF package and custom scripts in Python (https://github.com/cmccully/lcogtgemini/). We performed overscan and master bias subtraction and corrected for the quantum efficiency difference between the chips using Gemini IRAF tasks. We removed any remaining differences in the inter-pixel sensitivity from lamp flat field images. Pixels affected by cosmic rays were identified using the astroscrappy package (https://github.com/astropy/astroscrappy).

Note that given the distance of OGLE14-073, a time-dilation correction has been applied, and all the phases reported are always to be considered in rest-frame, unless explicitly expressed.

The host galaxy analyses were performed on pre-discovery ugriz images taken on 2012 December 22.33 UT by the DES during Science Verification. No flux from the supernova is assumed to have been present at this time. Magnitude measurements of the host were carried out using aperture photometry within IRAF/DAOPHOT. We let the aperture size vary until we were confident that it encompassed the whole host flux and avoided other nearby objects. The aperture radius adopted was around 2″. The zero point was determined with 55 reference stars in the field (~3′ around the host), which were also used for the supernova photometry calibration.

After the Milky Way extinction correction ($A_V = 0.17$ mag; ref. [47]), we applied the luminosity distance of 573.9 Mpc ($z = 0.1225$; ref. [48]) using a cosmology of $H_0 = 70\,\mathrm{km\,s^{-1}\,Mpc^{-1}}$, $\Omega_M = 0.27$ and $\Omega_\lambda = 0.73$ to calculate the host flux.

We employed the MAGPHYS stellar population model program of ref. [8] to estimate the stellar mass from the observed photometry of the host galaxy. This code employs a library of stellar evolution and population models from ref. [49] and adopts the galactic disc initial mass function of ref. [50]. MAGPHYS first found the best-fit galaxy model ($\chi^2_{\mathrm{red}} = 1.4$) and then calculated the probability density function over a range of model values, inferring the median of stellar mass of $10^{8.7}\,M_\odot$, and a $1\sigma$ range from $10^{8.5}$ to $10^{8.9}\,M_\odot$ for the host of OGLE14-073. This stellar mass is a few times greater than host galaxies of some superluminous supernovae with slowly fading lightcurves (for example, ref. [9]). Following the mass–metallicity relation, this implies a sub-solar metallicity for the host of OGLE14-073. We noticed some flux excess of the observed r band while comparing the best-fit model, which indicates that the host may have a strong contribution from [O III] lines, as is also confirmed by our last spectrum of OGLE14-073 (see Fig. 2a).

We used the spectrum at +115 d after maximum for measuring the emission line flux from the host galaxy (see Fig. 2a). The contamination from the supernova is strong and the H$\beta$ line is not detected. Hence, we used the N2 method[10] for the oxygen abundance. Given the close wavelengths of H$\alpha$ and [N II] lines, this has the advantage of being less affected by dust extinction. We inferred an oxygen abundance of $12 + \log(\mathrm{O/H}) = 8.36 \pm 0.10$ for the host galaxy of OGLE14-073, which is equal to half of the solar abundance (assuming a solar abundance of $12 + \log(\mathrm{O/H}) = 8.69$; ref. [51]). This estimate, together with the stellar mass previously inferred, is in good agreement with the mass–metallicity relation[11]. Nevertheless, a future pure, deep host spectrum is required to measure the host metallicity more accurately.

We also measured the star formation rate (SFR; ref. [52]) of the host galaxy from the H$\alpha$ luminosity ($2.41 \times 10^{39}\,\mathrm{erg\,s^{-1}}$) and then divided it by 1.6 assuming a Chabrier initial mass function. The SFR of the host is $>0.01\,M_\odot\,\mathrm{yr^{-1}}$, and the specific SFR (stellar mass/SFR) is $>0.02\,\mathrm{Gyr^{-1}}$. We point out that this is actually a lower limit, since we did not apply any internal dust extinction correction and the H$\alpha$ flux is contaminated by the supernova flux.

**Modelling procedure.** The ejected mass $M_{\mathrm{ej}}$, the progenitor radius at the explosion $R_0$ and the total (kinetic plus thermal) explosion energy $E$ of OGLE14-073 were estimated using a well-tested modelling procedure, which is described in refs [14,53]. This procedure includes hydrodynamical modelling of all the main supernova observables (that is, the bolometric light curve, evolution of line velocities and temperature at the photosphere), where $M_{\mathrm{ej}}$, $R_0$ and $E$ are derived from a simultaneous chi-squared fit of these observables to the model calculations. The full radiation hydro models were calculated using the code presented in refs [16,54]. This enabled simulation of the evolution of the physical properties of supernova ejecta and reproduction of the behaviour of the main supernova observables, from the breakout of the shock wave at the stellar surface to the radioactive decay phase. The radiative transfer was accurately treated at all optical depth regimes by coupling the radiation moment equations with the hydrodynamics equations. A fully implicit Lagrangian finite difference scheme was adopted to solve the energy and the radiation moment equations. The description of the ejecta evolution took into account the heating effects due to the decays of the radioactive isotopes synthesized during the supernova explosion. The gravitational effects of the compact remnant were also considered through a fully general-relativistic approach. The initial conditions used in the code well mimic the physical properties of a supernova progenitor after the shock breakout at the stellar surface and the reverse shock passage through the ejecta, with the exception of the outermost high-velocity shell of the supernova ejecta, which can recombine quickly and is not included. The outermost high-velocity shell of the supernova ejecta can provide a non-negligible contribution to the early emission of the supernova, preventing accurate reproduction of the evolution of the photospheric velocity in the early phases, but it is typically not crucial for the total mass–energy budget of the supernova. Including it would likely increase both the estimated ejected mass and explosion energy, reinforcing the idea that OGLE14-073 is an extraordinary object. In particular, the initial density profile is described by equation 6 of ref. [16]. This is derived from the so-called radiative zero solution of ref. [55] (which well approximates the initial temperature profile) assuming that the ejecta are radiation dominated.

However, the computation of a grid of models with the full radiation hydro code is very time consuming. Therefore, we need to first constrain the parameter space of the supernova progenitor and ejecta. This is accomplished by means of the semi-analytical model described in refs [15,53], which solves the energy balance equation for ejecta of constant density and free coasting (in homologous expansion). The plasma is assumed to be dominated by the radiation pressure. Both the recombination of the ionised matter and the decay of the $^{56}$Ni and $^{56}$Co synthesized during the explosion are considered as sources of heating of the ejecta. The parameter estimates were carried out as described above, fitting the main supernova observables to model calculations using $M_{\mathrm{ej}}$, $R_0$ and $E$ (or the initial expansion velocity) as fitting parameters. This preliminary analysis yielded $E = 21^{+29}_{-13} \times 10^{51}$ erg, $M_{\mathrm{ej}} = 69^{+52}_{-36}\,M_\odot$ and $R_0 = 3.5^{+0.8}_{-1.1} \times 10^{13}$ as the best parameters at a confidence level of $3\sigma$.

Once an approximate but reliable estimate of the physical conditions describing the supernova progenitor at the explosion was obtained, such a reduced framework was used as a start for the above-mentioned general-relativistic, radiation-hydrodynamics

Lagrangian modelling. The parameters resulting from this modelling were $E = 12.4^{+13.0}_{-5.9} \times 10^{51}$ erg, $M_{ej} = 60^{+42}_{-16}\ M_{\odot}$ and $R_0 = 3.8^{+0.8}_{-1.0} \times 10^{13}$ cm ($1\sigma$ confidence level). The reported uncertainties are an estimate of the errors related to the chi-squared fitting procedure used for the modelling, and are inferred following the same approach as described in ref. [14] but considering $1\sigma$ confidence intervals. Usually the typical values of these uncertainties are in the range ~10–30% (relative error) for conventional type II supernovae. However, the unique characteristics of OGLE14-073 inflated these uncertainties, providing wide bounds for the inferred parameters, nevertheless reflecting a reliable and solid range of values. We note in particular that the upper error for the energy is in the order of 100%, suggesting that it is more probable that the explosion was more energetic with respect to what we have inferred, rather than less energetic. We also point out that the inferred errors do not include possible systematic uncertainties linked to the input physics (for example, opacity treatment and the approximate initial condition of our models) nor uncertainties related to the assumptions made in evaluating the modelled observational quantities (for example, the adopted reddening, explosion epoch and distance modulus). Although the variations of the parameters $E$, $M_{ej}$ and $R_0$ due to these systematic uncertainties may not be negligible, they do not have a significant impact on the overall results (see also section 2.1 of ref. [14] and references therein for further details). In the case of OGLE14-073, they can produce a systematic increase in $E$ (and $M_{ej}$), reinforcing the idea that OGLE14-073 is an extraordinary object that defies the canonical neutrino-driven core-collapse paradigm.

The parameters inferred from the semi-analytical model and the more accurate hydrodynamical modelling are in good agreement. The explosion energy is approximately 70% higher in the semi-analytical mode because the latter does not take into account the ejecta acceleration that occurs in the first few days after explosion, which converts most of their internal energy into kinetic energy. To correctly reproduce the velocity profile, the semi-analytical code requires a larger initial velocity, hence leading to an overestimate of the initial kinetic and total explosion energy.

**Data availability.** The data that support the findings of this study are available from the corresponding author upon reasonable request. OGLE-IV data can be accessed from http://ogle.astrouw.edu.pl/ogle4/transients/. PESSTO data can be accessed from http://www.pessto.org. DES Science Verification data can be accessed from http://des.ncsa.illinois.edu/releases/sva1D. Las Cumbres Observatory images are available from http://lcogt.net/. Two Micron All Sky Survey data can be retrieved from http://www.ipac.caltech.edu/2mass/.

Received: 14 December 2016; Accepted: 26 July 2017;
Published online: 18 September 2017

## References

1. Richardson, D. et al. A comparative study of the absolute magnitude distributions of supernovae. *Astron. J.* **123**, 745–752 (2002).
2. Janka, H.-T. Explosion mechanisms of core-collapse supernovae. *Annu. Rev. Nucl. Part. Sci.* **62**, 407–451 (2012).
3. Wyrzykowski, Ł. et al. OGLE-IV real-time transient search. *Acta Astron.* **64**, 197–232 (2014).
4. Udalski, A., Szymański, M. K. & Szymański, G. OGLE-IV: fourth phase of the Optical Gravitational Lensing Experiment. *Acta Astron.* **65**, 1–38 (2015).
5. Blagorodnova, N. et al. PESSTO spectroscopic classification of optical transients. *The Astronomer's Telegram* **6489** (2014).
6. Smartt, S. J. et al. PESSTO: survey description and products from the first data release by the Public ESO Spectroscopic Survey of Transient Objects. *Astron. Astrophys.* **579**, A40 (2015).
7. Dark Energy Survey Collaboration. The Dark Energy Survey: more than dark energy—an overview. *Mon. Not. Roy. Astron. Soc.* **460**, 1270–1299 (2016).
8. Da Cunha, E., Charlot, S. & Elbaz, D. A simple model to interpret the ultraviolet, optical and infrared emission from galaxies. *Mon. Not. Roy. Astron. Soc.* **388**, 1595–1617 (2008).
9. Chen, T.-W. et al. The host galaxy and late-time evolution of the superluminous supernova PTF12dam. *Mon. Not. Roy. Astron. Soc.* **452**, 1567–1586 (2015).
10. Pettini, M. & Pagel, B. E. [OIII]/[NII] as an abundance indicator at high redshift. *Mon. Not. Roy. Astron. Soc.* **348**, L59–L63 (2004).
11. Kewley, L. J. & Ellison, S. L. Metallicity calibrations and the mass–metallicity relation for star-forming galaxies. *Astrophys. J.* **681**, 1183–1204 (2008).
12. Hamuy, M. & Suntzeff, N. B. SN 1987A in the LMC. III—UBVRI photometry at Cerro Tololo. *AJ* **99**, 1146–1158 (1990).
13. Hamuy, M. Observed and physical properties of core-collapse supernovae. *Astrophys. J.* **582**, 905–914 (2003).
14. Pumo, M. L. et al. Radiation-hydrodynamical modelling of underluminous type II plateau supernovae. *Mon. Not. Roy. Astron. Soc.* **464**, 3013–3020 (2017).
15. Zampieri, L. et al. Peculiar, low-luminosity type II supernovae: low-energy explosions in massive progenitors? *Mon. Not. Roy. Astron. Soc.* **338**, 711–716 (2003).
16. Pumo, M. L. & Zampieri, L. Radiation-hydrodynamical modeling of core-collapse supernovae: light curves and the evolution of photospheric velocity and temperature. *Astrophys. J.* **741**, 41 (2011).
17. Müller, B., Heger, A., Liptai, D. & Cameron, J. B. A simple approach to the supernova progenitor-explosion connection. *Mon. Not. Roy. Astron. Soc.* **460**, 742–764 (2016).
18. Nadyozhin, D. K. Explosion energies, nickel masses and distances of type II plateau supernovae. *Mon. Not. Roy. Astron. Soc.* **346**, 97–104 (2003).
19. Heger, A. & Woosley, S. E. The nucleosynthetic signature of population III. *Astrophys. J.* **567**, 532–543 (2002).
20. Dessart, L., Waldman, R., Livne, E., Hillier, D. J. & Blondin, S. Radiative properties of pair-instability supernova explosions. *Mon. Not. Roy. Astron. Soc.* **428**, 3227–3251 (2013).
21. Kozyreva, A., Blinnikov, S., Langer, N. & Yoon, S.-C. Observational properties of low-redshift pair instability supernovae. *Astron. Astrophys.* **565**, A70 (2014).
22. Woosley, S. E. Pulsational-pair instability supernovae. *Astrophys. J.* **836**, 244 (2017).
23. Dessart, L., Hillier, D. J., Audit, E., Livne, E. & Waldman, R. Models of interacting supernovae and their spectral diversity. *Mon. Not. Roy. Astron. Soc.* **458**, 2094–2121 (2016).
24. Arnett, W. D. On the theory of type I supernovae. *Astrophys. J.* **230**, L37–L40 (1979).
25. Galama, T. J. et al. An unusual supernova in the error box of the $\gamma$-ray burst of 25 April 1998. *Nature* **395**, 670–672 (1998).
26. Botticella, M. T. et al. Supernova 2009kf: an ultraviolet bright type IIP supernova discovered with Pan-STARRS 1 and GALEX. *Astrophys. J.* **717**, L52–L56 (2010).
27. Utrobin, V. P., Chugai, N. N. & Botticella, M. T. Type IIP supernova 2009kf: explosion driven by black hole accretion? *Astrophys. J.* **723**, L89–L92 (2010).
28. Taddia, F. et al. Long-rising type II supernovae from Palomar Transient Factory and Caltech Core-Collapse Project. *Astron. Astrophys.* **588**, A5 (2016).
29. Berger, E. et al. The spectroscopic classification and explosion properties of SN 2009nz associated with GRB 091127 at z = 0.490. *Astrophys. J.* **743**, 204 (2011).
30. Fraser, M. et al. SN 2009md: another faint supernova from a low-mass progenitor. *Mon. Not. Roy. Astron. Soc.* **417**, 1417–1433 (2011).
31. Kushnir, D. The progenitors of core-collapse supernovae suggest thermonuclear origin for the explosions. Preprint at https://arxiv.org/abs/1506.02655 (2015).
32. Thompson, T. A., Chang, P. & Quataert, E. Magnetar spin-down, hyperenergetic supernovae, and gamma-ray bursts. *Astrophys. J.* **611**, 380–393 (2004).
33. MacFadyen, A. I., Woosley, S. E. & Heger, A. Supernovae, jets, and collapsars. *Astrophys. J.* **550**, 410–425 (2001).
34. Gal-Yam, A. Luminous supernovae. *Science* **337**, 927 (2012).
35. Inserra, C. et al. Super-luminous type Ic supernovae: catching a magnetar by the tail. *Astrophys. J.* **770**, 128 (2013).
36. Kasen, D. & Bildsten, L. Supernova light curves powered by young magnetars. *Astrophys. J.* **717**, 245–249 (2010).
37. Smartt, S. J. Progenitors of core-collapse supernovae. *Annu. Rev. Astron. Astrophys.* **47**, 63–106 (2009).
38. Meynet, G. et al. Red supergiants, luminous blue variables and Wolf–Rayet stars: the single massive star perspective. *Bull. Soc. R. Sci. Liege* **80**, 266–278 (2011).
39. Vink, J. S., de Koter, A. & Lamers, H. J. L. Mass-loss predictions for O and B stars as a function of metallicity. *Astron. Astrophys.* **369**, 574–588 (2001).
40. Brown, T. M. et al. Las Cumbres Observatory Global Telescope Network. *Publ. Astron. Soc. Pac.* **125**, 1031–1055 (2013).
41. Valenti, S. et al. The diversity of type II supernova versus the similarity in their progenitors. *Mon. Not. Roy. Astron. Soc.* **459**, 3939–3962 (2016).
42. Cappellaro, E. SNOoPY: a package for supernova photometry (Padova-Asiago Supernova Group, 2014).
43. Stetson, P. B. DAOPHOT—a computer program for crowded-field stellar photometry. *Publ. Astron. Soc. Pac.* **99**, 191–222 (1987).
44. Landolt, A. U. UBVRI photometric standard stars in the magnitude range 11.5–16.0 around the celestial equator. *Astron. J.* **104**, 340–371 (1992).
45. Skrutskie, M. F. et al. The Two Micron All Sky Survey (2MASS). *Astron. J.* **131**, 1163–1183 (2006).
46. Chonis, T. S. & Gaskell, C. M. Setting UBVRI photometric zero-points using Sloan Digital Sky Survey ugriz magnitudes. *Astron. J.* **135**, 264–267 (2008).
47. Schlafly, E. F. & Finkbeiner, D. P. Measuring reddening with Sloan Digital Sky Survey stellar spectra and recalibrating SFD. *Astrophys. J.* **737**, 103 (2011).

48. Wright, E. L. A cosmology calculator for the world wide web. *Publ. Astron. Soc. Pac.* **118**, 1711–1715 (2006).
49. Bruzual, G. & Charlot, S. Stellar population synthesis at the resolution of 2003. *Mon. Not. Roy. Astron. Soc.* **344**, 1000–1028 (2003).
50. Chabrier, G. Galactic stellar and substellar initial mass function. *Publ. Astron. Soc. Pac.* **115**, 763–795 (2003).
51. Asplund, M., Grevesse, N., Sauval, A. J. & Scott, P. The chemical composition of the Sun. *Annu. Rev. Astron. Astrophys.* **47**, 481–522 (2009).
52. Kennicutt, R. C. Jr Star formation in galaxies along the Hubble sequence. *Annu. Rev. Astron. Astrophys.* **36**, 189–232 (1998).
53. Zampieri, L. in *The Multicolored Landscape of Compact Objects and Their Explosive Origins* (eds Di Salvo, T. et al.) 358–365 (2007).
54. Pumo, M. L., Zampieri, L. & Turatto, M. Numerical calculation of sub-luminous type II- plateau supernova events. *Mem. Soc. Astron. Ital. Suppl.* **14**, 123 (2010).
55. Arnett, W. D. Analytic solutions for light curves of supernovae of type II. *Astrophys. J.* **237**, 541–549 (1980).

## Acknowledgements

We thank M. Kubiak and G. Pietrzyn′ski—former members of the OGLE team—for contributions to the collection of the OGLE photometric data. G.T., S.B., E.C., N.E.-R., A.P. and M.T. are partially supported by PRIN–INAF 2014 with the project 'Transient Universe: unveiling new types of stellar explosions with PESSTO'. N.E.-R. acknowledges financial support from MIUR PRIN 2010–2011, 'The dark Universe and the cosmic evolution of baryons: from current surveys to Euclid'. G.T. is also supported by the fellowship for the study of bright type II supernovae, offered by INAF–OaPD. S.J.S. acknowledges funding from EU/FP7-ERC grant agreement 291222 and Science and Technology Facilities Council of the United Kingdom grants ST/I001123/1 and ST/L000709/1. T.-W.C. acknowledges support through the Sofia Kovalevskaja Award to P. Schady from the Alexander von Humboldt Foundation of Germany. T.J.M. is supported by the Grant-in-Aid for Research Activity Start-up of the Japan Society for the Promotion of Science (16H07413). F.T. and J.S. acknowledge support from the Knut and Alice Wallenberg Foundation. M.F. acknowledges support from a Royal Society—Science Foundation Ireland University Research Fellowship. Ł.W. was supported by the Polish National Science Centre grant OPUS 2015/17/B/ST9/03167. D.A.H. and C.M. are supported by NSF 1313484. G.D. and M.S. acknowledge support from EU/FP7-ERC grant 615929 and the Weizmann-UK 'Making Connections' programme. A.G.-Y. is supported by EU/FP7 via ERC grant 307260, the Quantum Universe I-Core programme by the Israeli Committee for planning and funding and the Israel Science Foundation, and Kimmel and YeS awards. A.J. acknowledges funding by the European Union's Framework Programme for Research and Innovation Horizon 2020 under Marie Sklodowska-Curie grant agreement 702538. K.M. acknowledges support from the Science and Technology Facilities Council of the United Kingdom through an Ernest Rutherford Fellowship. Z.K.-R. acknowledges support from ERC Consolidator Grant 647208. The OGLE project has received funding from the National Science Centre, Poland, grant MAESTRO 2014/14/A/ST9/00121 to A.U. This study is based on observations collected at the European Organisation for Astronomical Research in the Southern Hemisphere, Chile, as part of PESSTO (ESO programme IDs 197.D.1075, 191.D-0935 and 188.D-3003) and observations made with ESO telescopes at the Paranal Observatory under programme 096.D-0894(A). GEMINI spectra were obtained under the GS-2015A-Q-56 programme (Principal Investigator D.A.H.). We are grateful to the Istituto Nazionale di Fisica Nucleare—Laboratori Nazionali del Sud for the use of computer facilities. This project used public archival data from the DES. Funding for the DES projects was provided by the U.S. Department of Energy, U.S. National Science Foundation, Ministry of Science and Education of Spain, Science and Technology Facilities Council of the United Kingdom, Higher Education Funding Council for England, National Center for Supercomputing Applications at the University of Illinois at Urbana-Champaign, Kavli Institute for Cosmological Physics at the University of Chicago, Center of Cosmology and Astro Particle Physics at Ohio State University, Mitchell Institute for Fundamental Physics and Astronomy at Texas A&M University, Brazilian National Council for Scientific and Technological Development, Fundação de Amparo à Pesquisa do Estado do Rio de Janeiro, Financiadora de Estudos e Projetos, Ministry of Economy and Competitiveness (Spain), Deutsche Forschungsgemeinschaft (Germany) and the collaborating institutions in the DES, which are the Argonne National Laboratory, University of California Santa Cruz, University of Cambridge, Centro de Investigaciones Energéticas, Medioambientales y Technológicas in Madrid, University of Chicago, University College London, DES–Brazil Consortium, University of Edinburgh, ETH Zürich, Fermilab, University of Illinois, Institute of Space Sciences (Institute of Space Studies of Catalonia–Spanish National Research Council), Institute for High Energy Physics at the Universitat Autònoma de Barcelona, Lawrence Berkeley Laboratory, Ludwig Maximilian University of Munich and the associated Excellence Cluster Universe, University of Michigan, National Optical Astronomy Observatory, University of Nottingham, Ohio State University, University of Pennsylvania, University of Portsmouth, SLAC National Laboratory, Stanford University, University of Sussex and Texas A&M University. This paper is also based on observations from the Las Cumbres Observatory: we thank their staff for excellent assistance. IRAF is distributed by the National Optical Astronomy Observatory, which is operated by the Association of Universities for Research in Astronomy under cooperative agreement with the National Science Foundation.

## Author contributions

G.T. initiated and coordinated the project, managed the follow-up campaign, carried out the photometric and spectroscopic analyses and wrote the manuscript. M.L.P. provided the hydrodynamical modelling and contributed to the preparation of the manuscript. T.-W.C. performed the host galaxy analyses. T.J.M. proposed and investigated the PISN scenario. F.T. identified the similarities of the target with SN 1987A and suggested the scaling. L.D. highlighted the issues with the interpretation of PISN and proposed the colliding shells scenario. L.Z. performed the semi-analytical modelling as a preliminary step to the full hydrodynamical modelling. S.J.S. is the principal investigator of PESSTO, through which we gathered all the observations at NTT. S.J.S. and S.B. supervised G.T., helped to coordinate the project and contributed to preparing and editing the manuscript, including final proofreading. C.I. helped with the magnetar hypothesis. E.C. and A.P. helped with theoretical interpretations, providing during preparation of the manuscript. M.N. retrieved the PISN models and helped to perform a thorough comparison of them. M.F. provided constructive criticism during preparation of the manuscript. Ł.W. was the main interlocutor with the OGLE team, providing all the data. D.A.H. was the principal investigator of the GEMINI proposal granting time from which we obtained two spectra that were reduced by C.M. and S.V. G.D. obtained the NTT observations. K.M., M.S., K.W.S., O.Y. and D.R.Y. (the PESSTO builders) helped to coordinate the observations using the NTT and administered the aspects of the PESSTO campaign. J.P.A., M.D.V., N.E.-R., A.G.-Y., A.J., E.K., J.S. and M.T. provided useful comments and advice on the first draft of the manuscript. Z.K.-R., S.K., P.M., M.P., P.P., R.P., D.S., J.S., I.S., M.K.S., A.U. and K.U. were part of the OGLE team and helped to obtain the data.

## Competing interests

The authors declare no competing financial interests.

## Additional information

**Supplementary information** is available for this paper at doi:10.1038/s41550-017-0228-8.

**Reprints and permissions information** is available at www.nature.com/reprints.

**Correspondence and requests for materials** should be addressed to G.T.

**Publisher's note:** Springer Nature remains neutral with regard to jurisdictional claims in published maps and institutional affiliations.